Preliminary report on the M_w=6.9 Samos earthquake of 30 October 2020

P. Papadimitriou[1], V. Kapetanidis[1], A. Karakonstantis[1], I. Spingos[1], I. Kassaras[1], V. Sakkas[1], V. Kouskouna[1], A. Karatzetzou[2], K. Pavlou[1], G. Kaviris[1], N. Voulgaris[1]

[1] Section of Geophysics-Geothermics, Department of Geology and Geoenvironment, National Kapodistrian University of Athens, Panepistimiopolis 15784, Athens, Greece, ppapadim@geol.uoa.gr, vkapetan@geol.uoa.gr, akarakon@geol.uoa.gr, ispigos@geol.uoa.gr, kassaras@geol.uoa.gr, vsakkas@geol.uoa.gr, vkouskouna@geol.uoa.gr, kpavlou@geol.uoa.gr, gkaviris@geol.uoa.gr, voulgaris@geol.uoa.gr

[2] Department of Civil Engineering, Aristotle University of Thessaloniki, Greece, akaratze@civil.auth.gr

Abstract

On 30 October 2020 11:51 UTC, an M_w=6.9 earthquake struck the offshore region north of Samos Island, Greece, in the Gulf of Kuşadasi, causing two fatalities and 19 minor injuries at Samos Island while 115 casualties and over 1030 injuries have been reported in Western Turkey. Preliminary results indicate that the mainshock occurred on a north-dipping normal fault, with φ=270º, δ=50º, λ=-81º. The selection of the nodal plane is supported by evidence of uplift at the western part of Samos Island, belonging to the footwall, and over 10cm of subsidence at the northernmost edge of the central part of the island. The relocated distribution of hypocenters shows clustering of events in a dense spatial group, east of the mainshock's epicenter, where most major aftershocks have occurred, while west of the mainshock a smaller group of aftershocks is observed, separated by a gap where few events are located. The latter is likely related to the region of the fault plane where most of the co-seismic slip occurred, with Coulomb stress-transfer towards the western and eastern margins of the rupture triggering aftershock activity. The possibly complex source time function of the mainshock that was observed during the preliminary processing of its waveforms indicate that it may have ruptured more than one structures, which could also explain the relatively low magnitude of the largest aftershock (M_w=5.0). The mainshock caused damage mainly to non-engineered constructions, i.e. old residential buildings, churches and monuments in Samos Island, and minor damage to the majority of the building stock of the island built under the restrictions of the National seismic code. On the other hand, it caused severe damage at Izmir, especially to high-rise buildings. The mainshock also triggered a small tsunami that reached heights of over 1 m, mainly at the Turkish coast.

1. Introduction

The Aegean Sea is one of the most seismically active areas in the SE Mediterranean. The western extension of the North Anatolian Fault, to the north, and the Hellenic Trench, to the south, bound the Aegean microplate (McKenzie, 1978; Mercier *et al.*, 1989). Tectonics in the northern Aegean are dominated by dextral strike-slip faulting along NE-SW striking structures, parallel to the North Aegean Trough (NAT), while conjugate sinistral strike-slip faulting is also present, associated to certain large events (e.g. the 26 July 2001 *M* = 6.3 and the 3 April 1967 *M* = 6.7 earthquakes near Skyros Island; McKenzie, 1972; Karakostas *et al.*, 2003; Roumelioti *et al.*, 2003). The tectonic environment around the eastern Aegean strongly differs; E-W striking faults close to the Greek islands (such as Samos) and the Western Turkish shores exhibit oblique-normal motions. These localized systems are closely related to minor basins and gulfs around the Greek-Turkish border, as in the cases of Lesvos-Edremit (Kurtuluş *et al.*, 2009), Samos-Kuşadasi (Tan *et al.*, 2014) and Gökova (Gürer *et al.*, 2013).

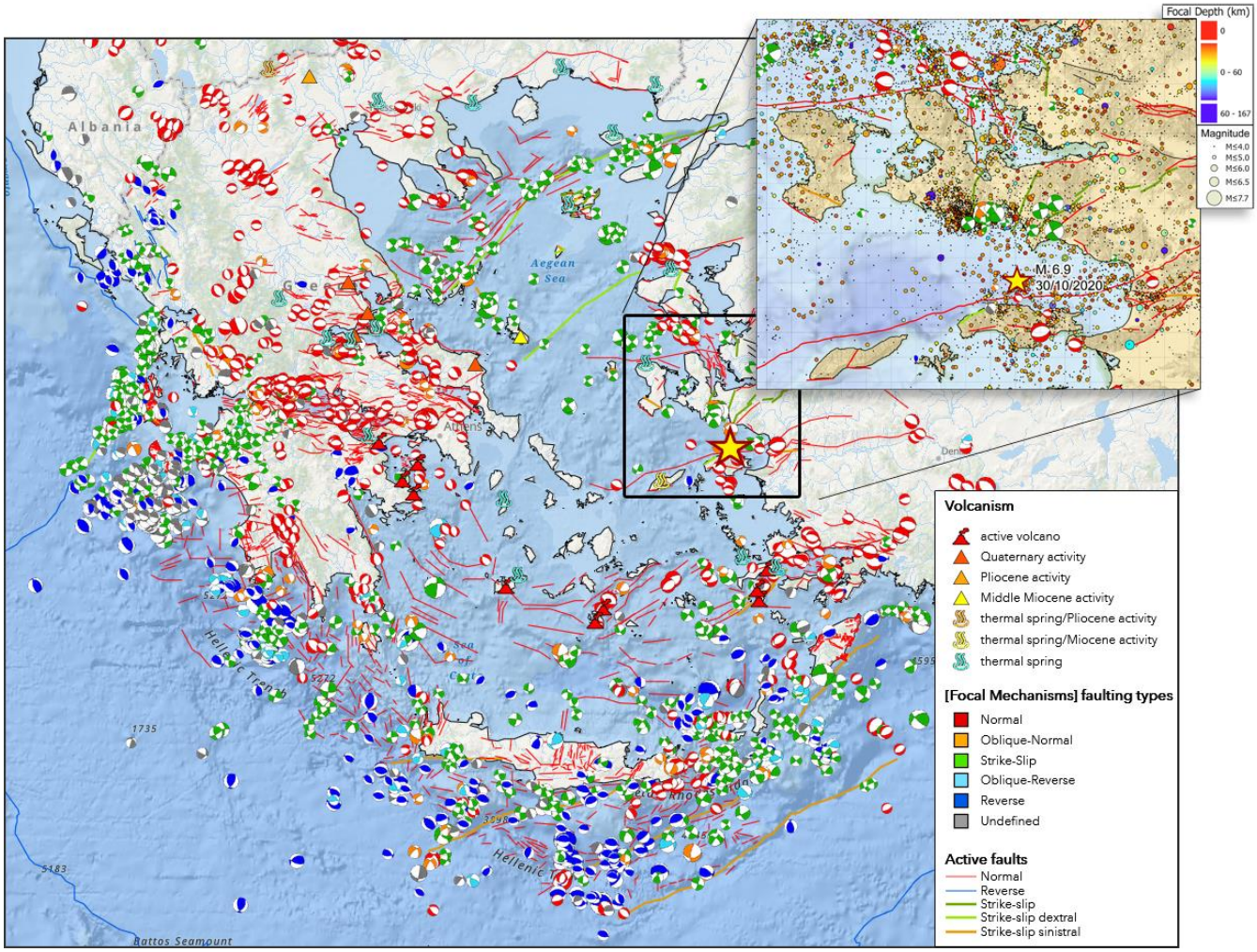

Figure 1: Snapshot from the New Seismotectonic Atlas of Greece v1.0 (Kassaras *et al.*, 2020), presenting focal mechanisms (period 1995 – June 2020, by SL-NKUA) and active faults (NOAFAULTs, Ganas *et al.*, 2018), coloured by faulting type, along with volcanism and hydrothermal activity. The epicenter of the October 30th 2020 mainshock is presented by a yellow star. Inset map: past instrumental seismicity (1901-June 2020; from the compilation of Kassaras *et al.*, 2020) and focal mechanisms of significant earthquakes at crustal depths (from the compilation of Kapetanidis & Kassaras, 2019) in the broader region of the 2020 Samos earthquake. The interactive GIS web application of the New Seismotectonic Atlas of Greece v1.0 is available at the following link: http://www.geophysics.geol.uoa.gr/atlas.html

The broader area of the eastern Aegean Sea (Fig. 1) is part of a transition zone of deformation, with a width in the order of 100 km (e.g. Papazachos, 1999). GPS measurements indicate that the anomalously low extension rate, compared to the elevated values that prevail in the Aegean, allows the Anatolia microplate to move with increasing velocity to the WSW, leading to the westward opening of the Izmir Bay (e.g. Mascle and Martin, 1990). The deformation that occurs in the onshore part of western Turkey features N-S striking crustal extension, evidenced by numerous earthquakes located along the Inner İzmir Bay Basin and the Gulf of Kuşadasi (Genç *et al.*, 2001). Nevertheless, there are also scarce occurrences of strike-slip faulting in the broader area of Karaburun peninsula (e.g. Ocakoğlu *et al.*, 2004).

On 30/10/2020 11:51 UTC, an M_w=6.9 earthquake occurred in the offshore area north of Samos Island, in the Gulf of Kuşadasi (Fig. 1). Two fatalities and 19 minor injuries were reported at Samos Island, along

with several injuries and significant damage to the building stock. In Western Turkey, the effects of the event were detrimental, with 115 fatalities, over 1030 injuries and structural damage that included collapses. A minor tsunami was also reported.

2. Geology and tectonics of Samos Island

Samos is a largely mountainous Greek island, approximately 1.5 km away from the Turkish shore in the east. It hosts several areas of economic interest, such as Karlovasi to the northwest and Vathy (also named "Samos") to the northeast (Fig. 2). The island's population is 33,814, which makes it the 9th most populous of the Greek islands. Samos' mountains are an extension of the Mycale range on the Anatolian mainland. The geology of the island consists of a number of metamorphic nappes, a non-metamorphic nappe and Miocene graben. Because of the quite complicated geology (Fig. 2), the island offers a look on an exceptionally complete nappe stack of the Central Hellenides, ranging from the high-pressure metamorphosed Basal Unit (as part of the External Hellenides) all the way up to the ophiolitic Sélcuk nappe and the non-metamorphosed Cycladic ophiolite nappe (Pomonis & Hatzipanagiotou, 1998; Ring *et al.*, 2007; Jolivet & Brun 2010; Malandri *et al.*, 2017).

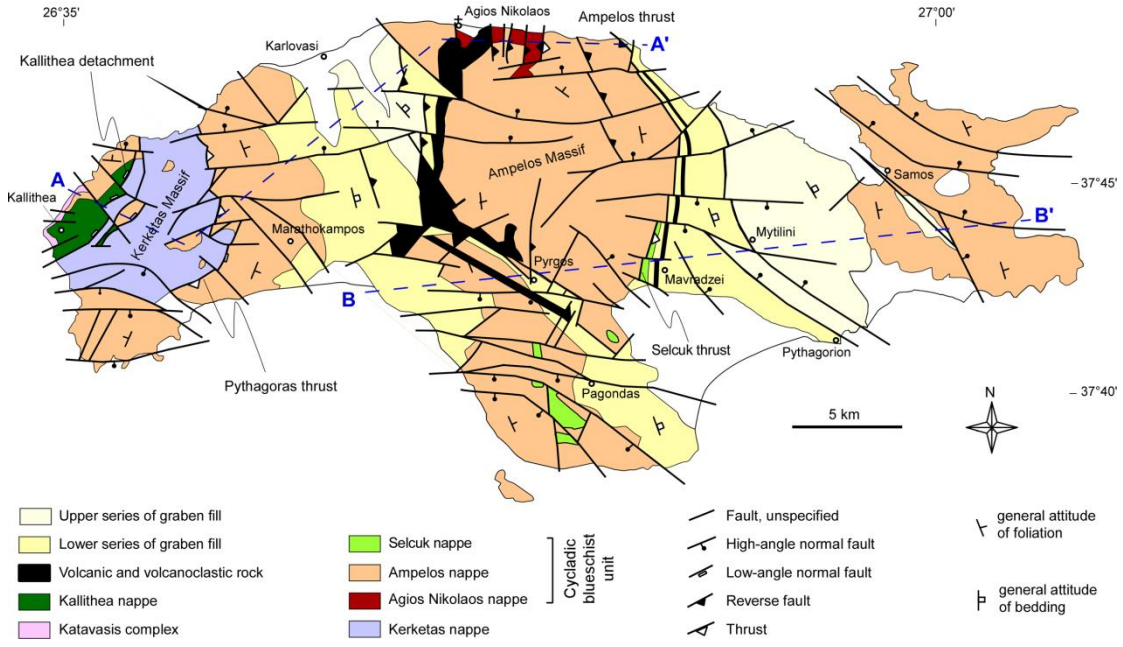

Figure 2: Geologic map of Samos Island (modified by Ring *et al.*, 2007)

3. Past seismic activity in the region – Historical Data

The seismic history of Samos dates back to the 2nd century BC. Around 201-197 BC, an earthquake caused injuries among the people of the island of Samos. Over 200 years later, circa 46-47 AD, according to an inscription from Samos, in AD 47 the emperor Claudius restored the temple of Dionysus, which had collapsed because of age and an earthquake (Ambraseys, 2009).

Until the 18th century, no records on earthquake activity have been reported from Samos. In the Eastern Aegean islands but also on the opposite coasts of Asia Minor, poverty, fear and uncertainty prevail. The situation in the area is such that forces the Samians, in the summer of 1476, to migrate to Chios, with the immediate result of the complete desolation of Samos. In the period 1700-1799, eight damaging earthquakes with epicentres in the eastern Aegean affected Samos. Particularly the 18 June 1751 event destroyed many houses in the eastern part of the island and in the region of Kusadasi, causing great losses.

In the 19th century, ample information on seismicity is retrieved from the newspaper "Samos", published by Epameinontas Stamatiadis, who noted the seismic activity of the island in detail (Taxeidis, 2003). A total of 416 earthquakes have been reported as damaging or felt in Samos (Kouskouna & Sakkas, 2013). Structural damage and partial collapse to the buildings (Intensity I≥7) was caused by 14 of these events, mainly in the second half of the century. Furthermore, 11 events produced non-structural damage (Intensity 7>I≥6), with the rest being strongly felt with negligible damage or perceptible.

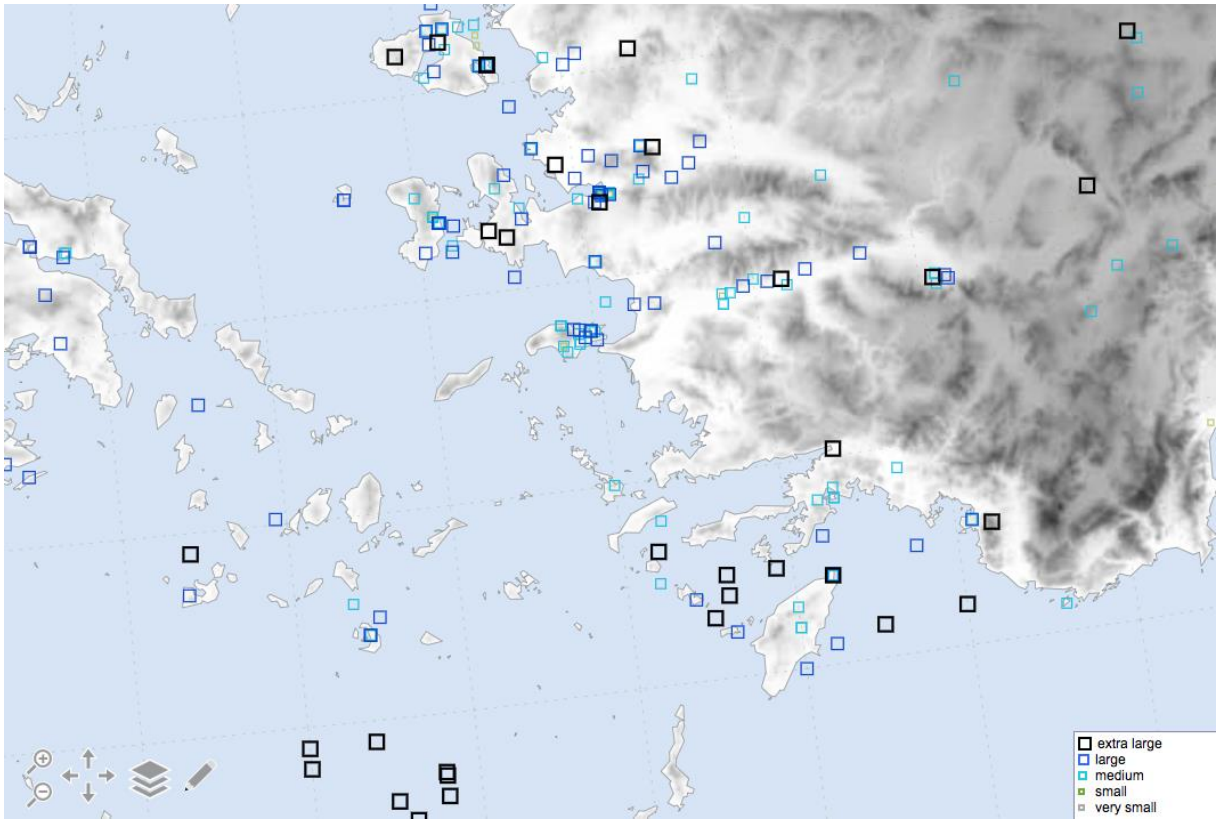

Figure 3: Historical seismicity of the broader Samos area in the period 1000-1899, as presented in AHEAD (Locati *et al.*, 2014).

The parameters of these earthquakes are assessed in many parametric catalogues (Papazachos & Papazachou, 2003; Taxeidis, 2003; Stucchi *et al.*, 2013), mainly based on macroseismic intensity data distribution inversion techniques, e.g. the "boxer" method by Gasperini *et al.* (2010) in the SHEEC catalogue of Stucchi *et al.* (2013). The distribution of macroseismic data points, as well the epicentre of each earthquake, are included in the Hellenic Macroseismic database (Kouskouna and Sakkas 2013; http://macroseismology.geol.uoa.gr/query_eq/) and the AHEAD database (Locati *et al.*, 2014; Fig. 3).

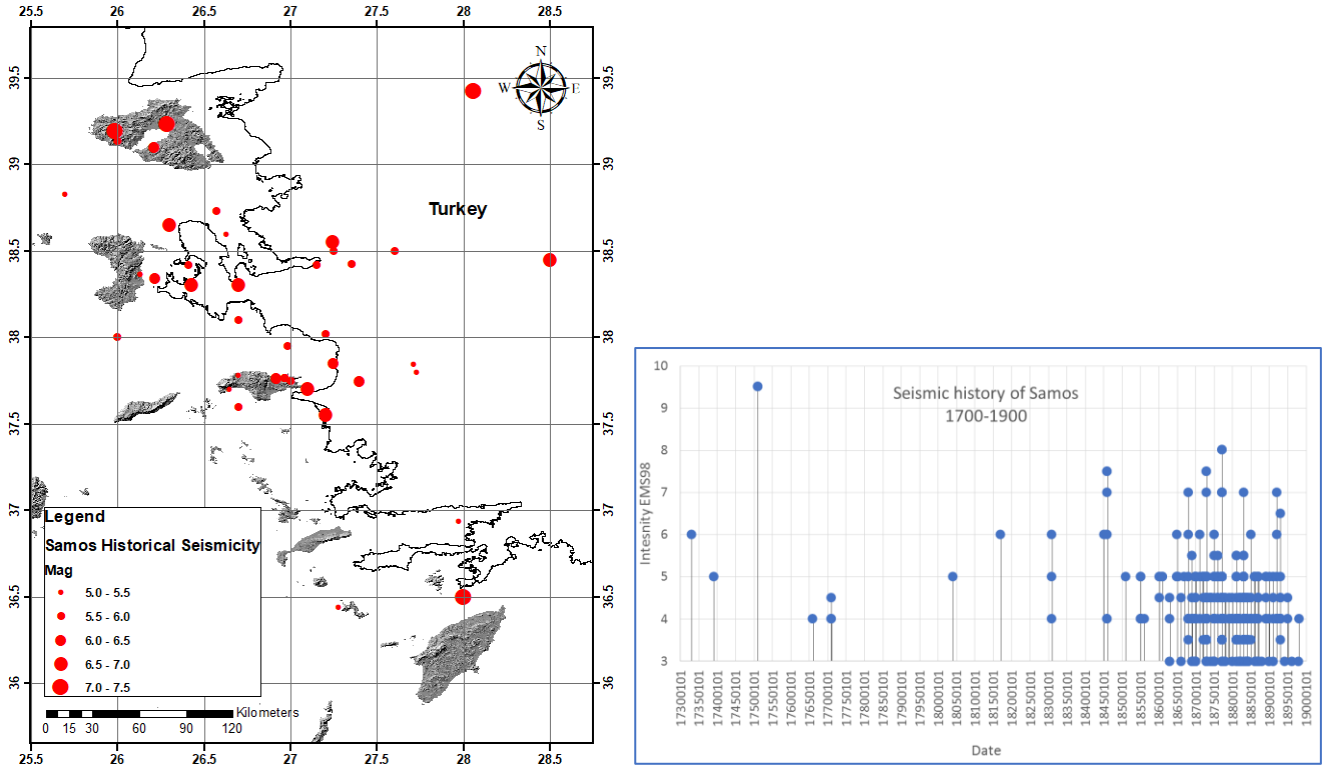

Figure 4: (Left) Epicentral distribution of historical earthquakes with M≥5.0 in the broader Samos area during the period 1000-1899. (Right) The seismic history of Samos in the period 1700-1900, in terms of assigned EMS98 intensity (Taxeidis 2003, Kouskouna and Sakkas 2013).

The historical earthquake magnitudes are equivalent moment magnitudes, estimated using macroseismic data. For the events with more than 10 macroseismic intensity data points, the "Boxer" method was applied (Gasperini *et al.*, 2010) and for those with few intensity data points a local empirical relationship was used (Taxeidis, 2003). The estimated magnitudes were found in the range of 3.9-7.3 (Fig. 4), with a number of 46 events with magnitudes greater than 5.0. The magnitude uncertainties of such estimations may reach the value of ±0.5.

In the early 20th century, an earthquake on 11 August 1904 (Fig. 5) with estimated equivalent moment magnitude M_w=6.1, is considered the most damaging event in Samos. Its epicentre was located off the south coast of Samos, at the time an independent principality, causing widespread damage. The mainshock and its larger aftershocks ruined the villages of Marathokampos, Konteika, Kaminia, Kumeika, Pyrgos, Skureika, the monastery of St. Trianta and Hora with some loss of life. At Hora, out of 650, mostly old houses, 208 were totally destroyed, 400 were ruined, four people were killed and 15 injured. At Marathokampos and Pyrgos all public buildings, including the churches, were damaged beyond repair and quite a few of them collapsed. Also at Tigani damage was considerable, particularly to the quay of the port, which was irreparable. At Vathy the upper part of the town was damaged more than the lower with no loss of life. Damage in the north part of the island at Karlovasi and lower Vathy was minor with only one house collapsed and 50 damaged.

The macroseismic reports of these past events predicate knowledge on the geometry and kinematics of the activated faults (e.g. Papazachos & Papazachou 2003; Tan *et al.*, 2014; Kouskouna *et al.*, 2012). The macroseismic reports seem to be well-correlated with the effects produced by the recent event that took place north of Samos Island.

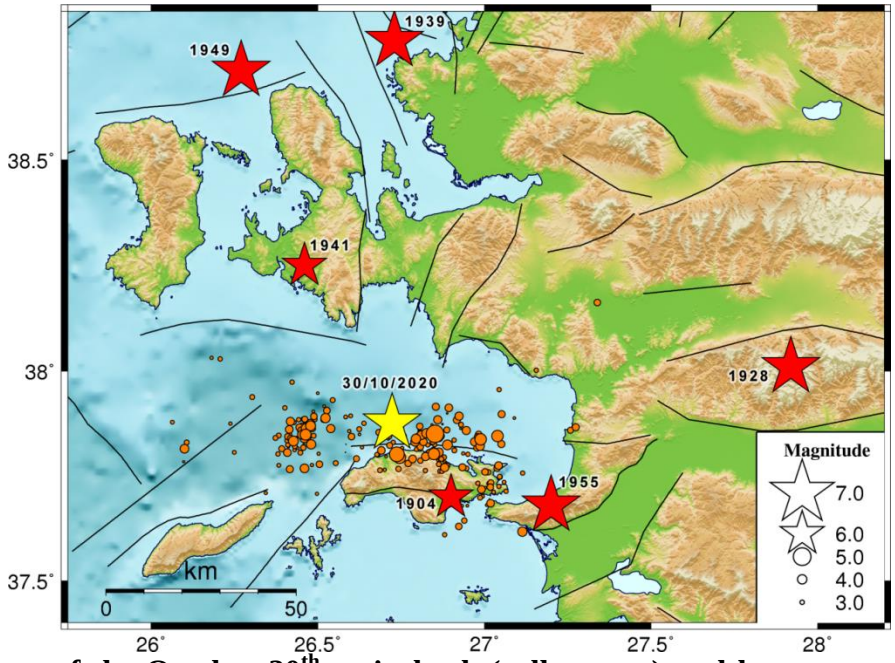

Figure 5: Epicenter of the October 30th mainshock (yellow star) and large events ($M_w \geq 6.0$) of the instrumental era (red stars) of the broader area of study (from the catalogue of Makropoulos *et al.*, 2012). Orange circles depict the manually located epicenters of the 2020 Samos aftershocks.

4. The 2020 Samos mainshock

4.1. Focal mechanism of the mainshock

Regarding the focal mechanism of the 30/10/2020 Samos mainshock, we adopted a processing scheme which incorporates regional moment tensor inversion. Green functions were computed with the frequency-wavenumber integration method (Bouchon, 1979, 2003). Next, synthetic waveforms were generated and compared with the observed ones, following the procedure proposed by Papadimitriou *et al.* (2012). The aforementioned method has been successfully applied in several case studies in Greece, e.g. Santorini during the 2011-2012 seismic crisis (Papadimitriou *et al.*, 2015; Kaviris *et al.*, 2015), Lesvos Island, where a normal fault was activated in 2017 (Papadimitriou *et al.*, 2018) and Zakynthos Island, where a low-angle strike-slip fault generated an M_w=6.7 mainshock (Papadimitriou *et al.*, 2020).

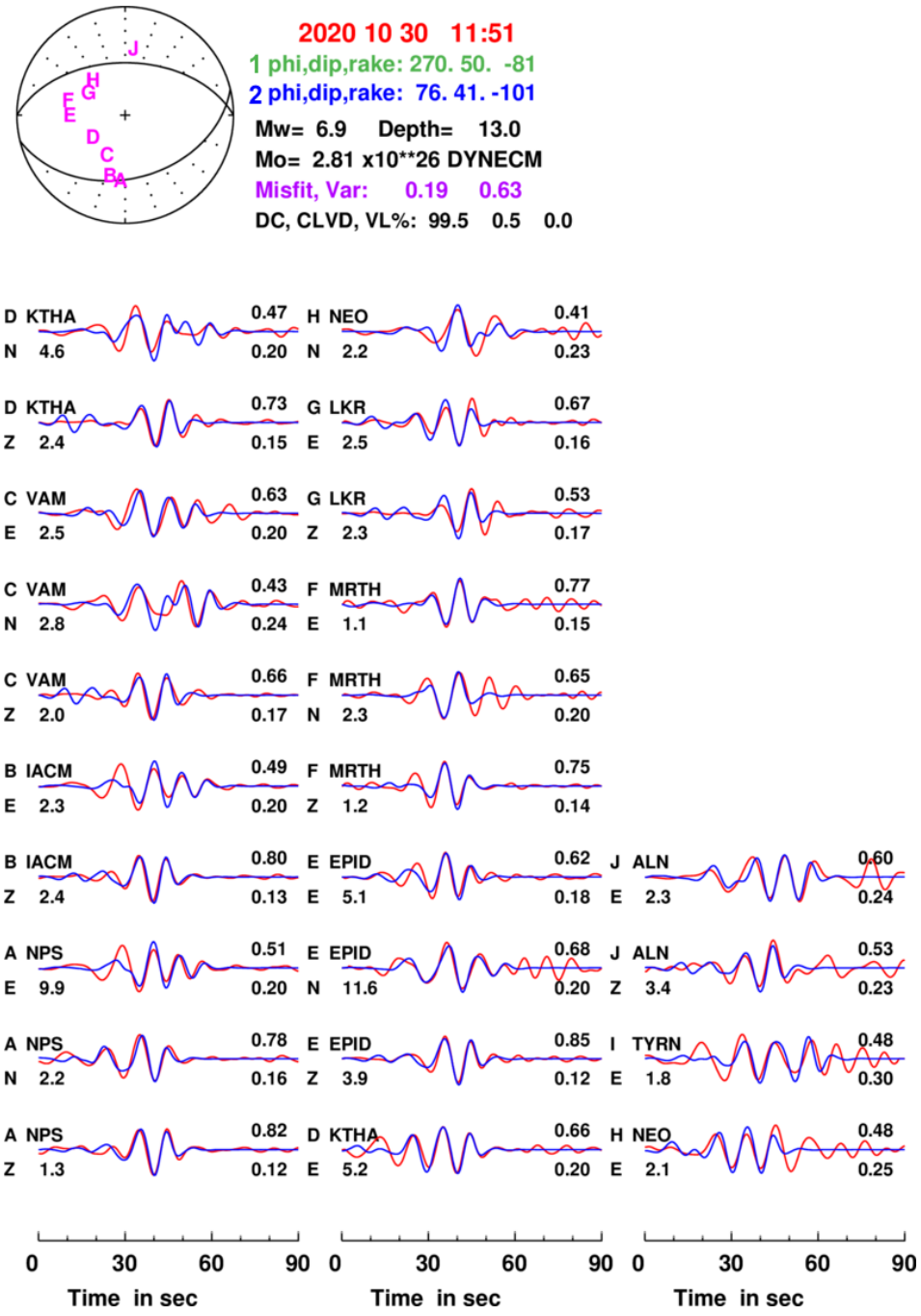

Figure 6: Results of the focal mechanism determination for the mainshock. The focal mechanism (top), along with key information (including two quality criteria, i.e. misfit and variance reduction) about the solution are shown. The comparison between observed (red) and synthetic (blue) waveforms is also presented, offering further insight about the reliability of the solution. For each waveform subfigure, the following information is shown (clockwise from top left); the position of the station on the focal sphere (A-J), the station code, the variance reduction, the misfit, the individual seismic moment (in units of 10^{26} dyn·cm) and the component code (i.e. Z for vertical, E for E-W and N for N-S).

Based on the above-mentioned methodology, the source parameters of both the mainshock and the major aftershocks of the sequence were determined. The mainshock of the Samos sequence occurred on 30/10/2020 11:51:28 UTC. The geographical coordinates of the epicenter are 37.8759ºN and 26.7235ºE. A quite satisfactory fault-plane solution has been obtained (Fig. 6), considering some observed indications that the source time function appears to be complex. Teleseismic modeling will be required for more detailed results. The mainshock, with a centroid depth of 13.0 km, produced seismic moment equal to $M_0=2.81\cdot10^{26}$ dyn·cm. Thus, the moment tensor inversion yielded a slightly stronger earthquake magnitude ($M_w=6.9$), compared to that obtained through routine analysis ($M_L=6.7$). The determined focal mechanism indicates normal faulting with the fault plane oriented in an almost E-W direction ($\varphi_1=270º$, $\delta_1=50º$, $\lambda_1=-81º$ and $\varphi_2=76º$, $\delta_2=41º$, $\lambda_2=-101º$).

4.2. Ground deformation

Interferometric processing was performed in an initial attempt to study the co-seismic ground deformation due to the 30/10/2020 mainshock on Samos Island. Satellite radar images from the SENTINEL 1A and 1B constellation were processed using ESA's platform "geohazards TEP" (https://geohazards-tep.eu/). The SNAP algorithm was adopted for the differential interferometric processing. Two pairs of radar images were processed, one on *ascending* and the other on *descending* orbital geometry.

For the *ascending* orbital geometry, the time span for the two radar images was 6 days: October 24th to October 30th, with an incident angle of ~36.8°. The slave image (October 30th), was acquired just few hours after the main event. As a result, the observed deformation describes mainly the co-seismic motion and not contingent post-seismic effects. For the *descending* orbital geometry, the time span was 12 days: October 24th to November 5th. The phase of the differential interferograms was unwrapped and the Line Of Sight (LOS) displacement maps were produced (Fig. 7), presenting the ground displacement in metric units (m).

For both orbital geometries, the LOS displacement maps indicate that intense deformation occurred mainly in the northern and western part of the island, i.e. the areas closer to the mainshock's epicentre, while the eastern part exhibits quite smaller amplitudes of LOS displacement. The most prominent feature of the observed deformation is the intense positive LOS displacement values in the western part of the island (motion towards the satellite) for both acquisition geometries. The latter is consistent to the normal faulting motion of the uplifted footwall in the activated seismic fault, taking into consideration that the main motion component of the LOS vector is the vertical one and both geometries resulted to similar positive LOS displacement values. Nevertheless, there is a narrow coastal zone in the northern central part of the island where increased negative LOS displacement values (<-10cm; motion away from satellite) were observed. Moreover, the ascending acquisition geometry revealed a different type of motion at the eastern part of Samos with significantly smaller and negative LOS displacement values, indicating a differential motion between the eastern and western part of the island. However, this is not the case for the descending orbital geometry, where in the eastern part the LOS displacement is significantly smaller compared to the western one, but the values retain a positive sign.

In conclusion, it has to be stated that the overall deformation image of the island reveals a type of kinematic discontinuity in the central part of Samos. This feature differentiates the co-seismic motion between the western part (with high positive LOS displacement values) and the eastern part (quite smaller and even negative LOS displacement values in the ascending orbital geometry). Further investigation of the local tectonics and numerical modelling of the seismogenic fault is required in order to explain this phenomenon, associated with the geotectonic status of the area.

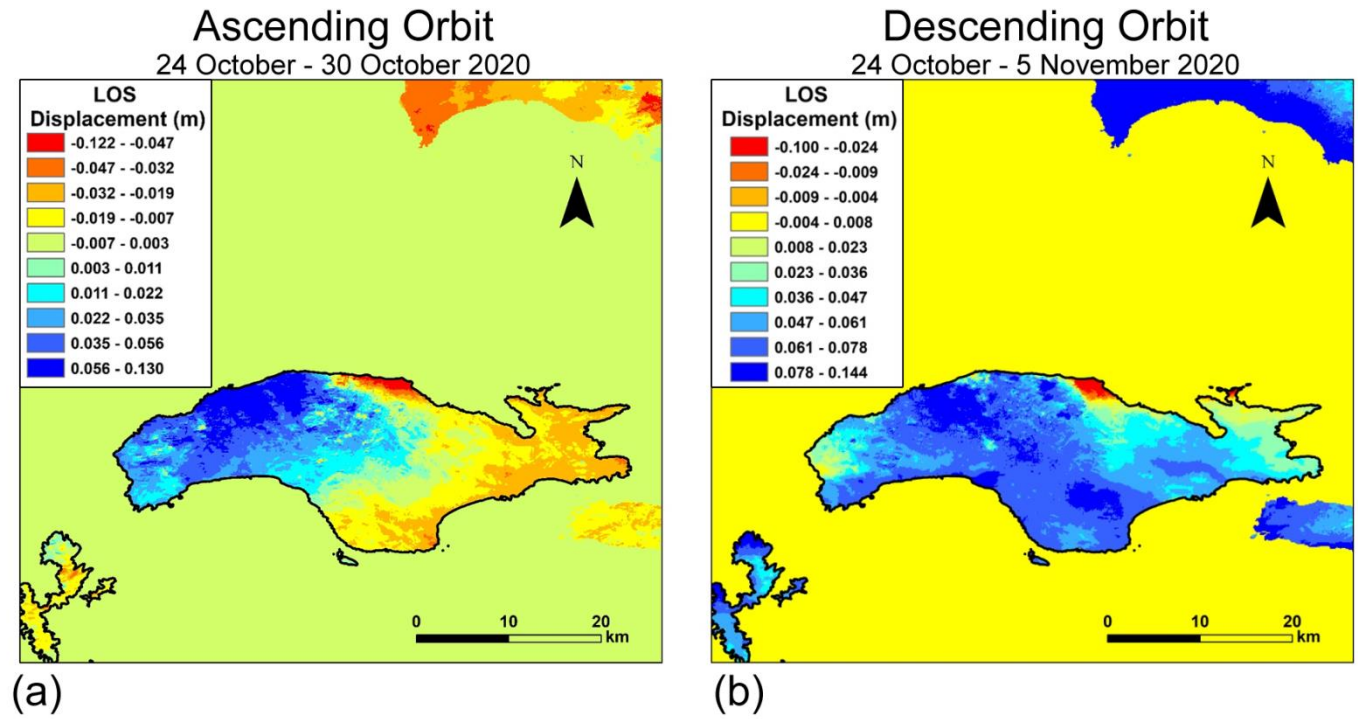

Figure 7. LOS Displacement maps of Samos Island deduced from interferometric processing of SENTINEL 1A and 1B radar images (a) for *ascending* orbit (24 – 30 October, 2020) and (b) for *descending* orbit (24 October – 5 November, 2020).

4.3. Shakemaps from instrumental and crowdsourcing data

Shakemaps (USGS, 2017) depict the distribution and severity of ground shaking, information that is critical for assessing the extent of the areas affected to determine which regions are potentially hit the hardest, allowing for a rapid estimation of losses. Fig. 8a presents the ShakeMap automatically generated for the 2020 Samos M_w=6.9 mainshock (more in the event's special page at the following link: http://www.geophysics.geol.uoa.gr/stations/gmaps3/eventpage_leaf.php?evid=2020-10-30-11-51-26&lng=en). The maximum observed intensity values reach VII at the northern part of Samos Island and the opposite coast of Turkey. To improve the ShakeMap, we also considered employing intensity data from testimonies of people who felt the earthquake. LastQuake (https://m.emsc.eu/) is a system at the intersection between seismology, citizen science and digital communication. Its aim is to offer timely, appropriate information in regions where an earthquake has been felt and to collect high numbers of eyewitnesses' direct and indirect observations about the degree of shaking being felt and possible damage incurred (Bossu et al., 2018). This improves rapid situation awareness and augments data at low cost. The resulting intensities after the incorporation of LastQuake data (Fig. 8b) significantly increase with respect to the theoretically expected ones (Fig. 8a).

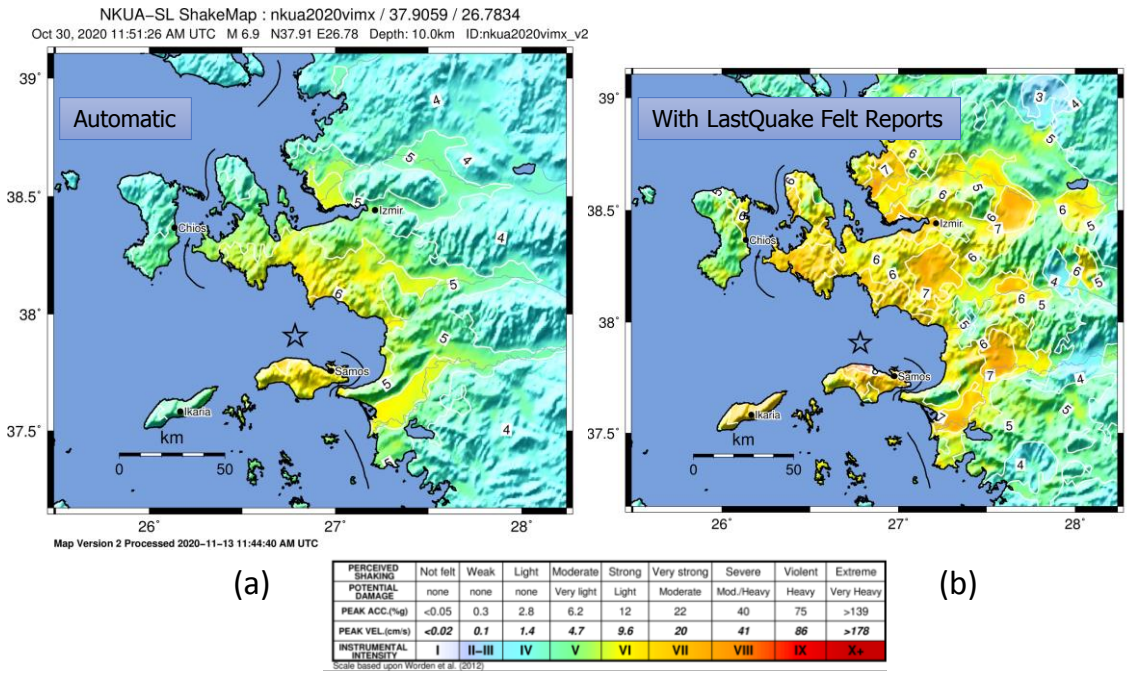

Figure 8. (a) Automatically generated ShakeMap (USGS, 2017) for the 2020 Samos M_w=6.9 mainshock using ground motion prediction equations and V_{S30} theoretical estimates from topography through the Allen & Wald (2009) approach; (b) with additional information from the EMSC felt reports (https://m.emsc.eu/).

5. Preliminary results for the 2020 Samos aftershock sequence

5.1. Relocation and spatiotemporal analysis

During the period between 30/10/2020 and 08/11/2020, a total of 232 events of the 2020 Samos sequence were detected and manually analysed at the Seismological Laboratory of the National and Kapodistrian University of Athens (SL-NKUA). We also collected catalogue and arrival-time data from the Geodynamics Institute of the National Observatory of Athens (GI-NOA) and compiled a merged catalogue of 367 events. In addition, we incorporated P and S arrival-time data for these events from stations installed in Turkey, as reported in the bulletin of the Turkish Disaster and Emergency Management Presidency (AFAD; https://deprem.afad.gov.tr).

We located the hypocenters using the HypoInverse code (Klein, 2002) and a custom velocity model that was constructed for this sequence, starting with a 1D model for the region of Karaburun (Erythres), Turkey (Karakonstantis, 2017). Although the aftershocks were located at the eastern margins of the Hellenic Unified Seismological Network (HUSN), the integration of data from stations located at Turkey achieved a satisfactory average azimuthal gap of 68°, with less than 100° for most events. However, the lack of data from local stations, especially during the first days of the sequence, limited the capability to constrain focal depths and resolve the geometries of the activated structures from the distribution of hypocenters. Furthermore, this caused hypocenters to be strongly affected by the selection of the velocity model, which could only be considered as preliminary.

To improve the relative locations of hypocenters, we have relocated the sequence using the HypoDD code (Waldhauser, 2001). This algorithm reduces uncertainties caused by discrepancies between the 1D velocity model and the real structure by minimizing the double difference between calculated and observed travel-times for pairs of neighboring events. To this purpose, we also incorporated waveform cross-correlation data from available stations in the region. Fig. 9 presents the preliminary relocation results. During the first days of the sequence, local data were mainly available from the accelerometric station KRL1, while data from the permanent station SMG and the temporary stations SAM1 and SAM2 of GI-NOA were available for events that occurred after a few days, in early November 2020. Waveform data from stations at the coasts of Turkey were also incorporated for the relocation procedure.

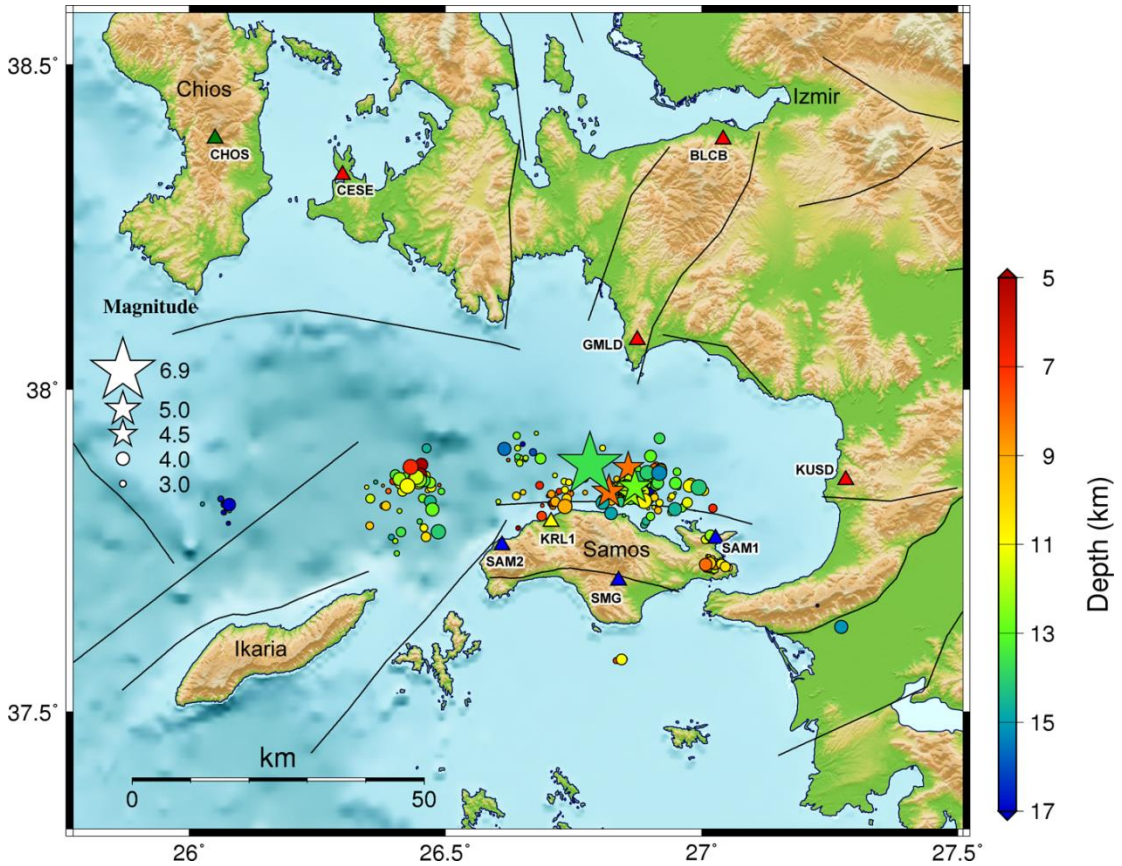

Figure 9: Preliminary relocation of the 2020 Samos aftershock sequence for the period between 30 October and 8 November 2020. The locations of available stations in the region are presented by triangles (Network codes: blue=HL, yellow=HI, green=HT, red=KO). The major events with M≥4.5 are depicted by stars.

The preliminary results for the 2020 aftershock sequence reveal the existence of several distinct spatial clusters (Fig. 10). The epicenter of the mainshock is located about 10 km N of the northern coast of Samos Island. A dense cluster of aftershocks (group 1, red) has occurred east of the mainshock. This is associated with the major aftershocks ($M_w \geq 4.5$, stars in Fig. 10) that have been reported for this sequence. The largest aftershock was an M_w=5.0 event that occurred on 30 October 2020, 15:14:57 UTC in group 1. An approximately 20-km-long area with very sparse to no seismicity can be observed west of the mainshock, with only few aftershocks in group 2 (green). Further west, a significant cluster of events is observed (group 3), while two additional, smaller, isolated clusters were also located, one at the eastern tip of Samos Island (group 4, cyan) and another to the north of Ikaria Island (group 5, yellow). Cross-

sections were performed in both a S-N (Fig. 11, a_1-a_2, b_1-b_2) and a W-E direction (c_1-c_2) to depict the distribution of hypocenters at depth. Most seismicity is located in a range of focal depths between 10 and 15 km. Although no clear planar geometries can yet be resolved from the hypocenters, their distribution in groups 1 and 2 along with the hypocenter of the mainshock is consistent with a north-dipping (at 50°) fault plane, outcropping near the northern coast of Samos Island (Fig. 11, profile b_1-b_2, dashed line). The latter result is consistent with reported preliminary deformation observations, showing subsidence at the northern tip of Samos Island and mainly uplift to its western part (see Section 4.2).

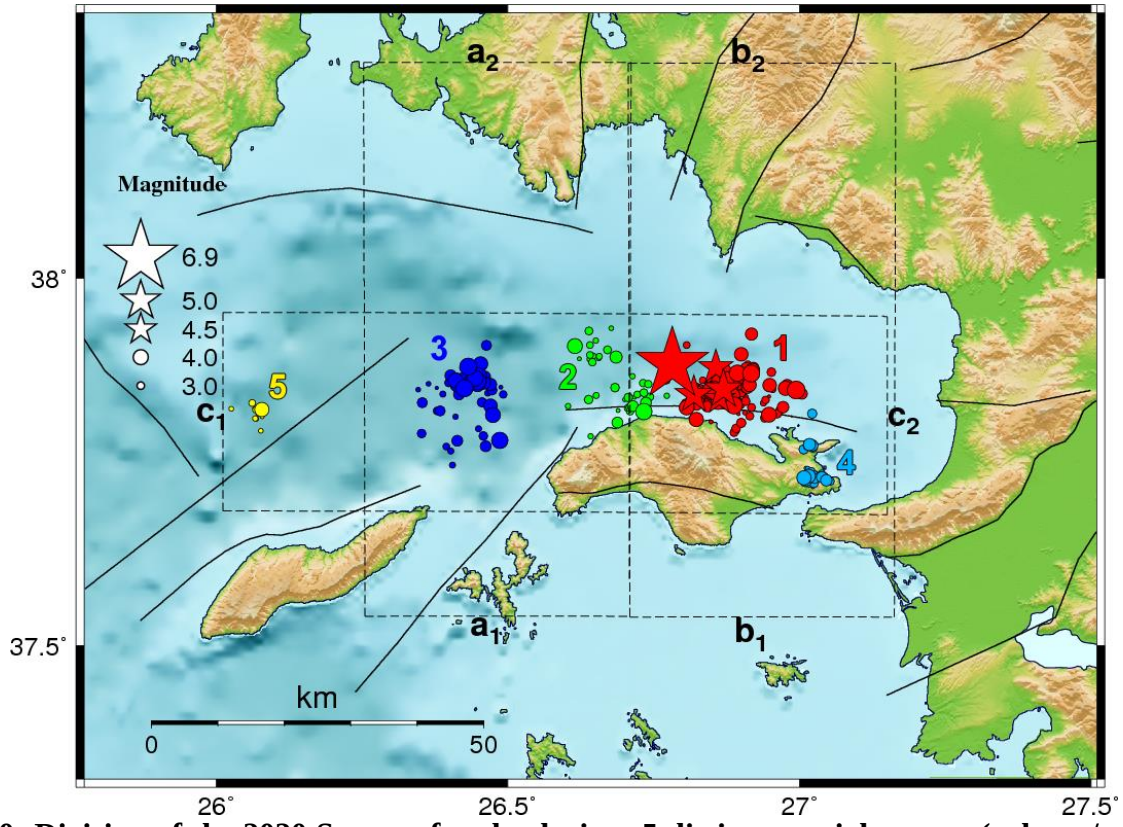

Figure 10: Division of the 2020 Samos aftershocks into 5 distinct spatial groups (colours/number in the map). The major events with M≥4.5 are depicted by stars. Dashed rectangles with a-c labels represent the direction and limits for the cross-sections of Fig. 11.

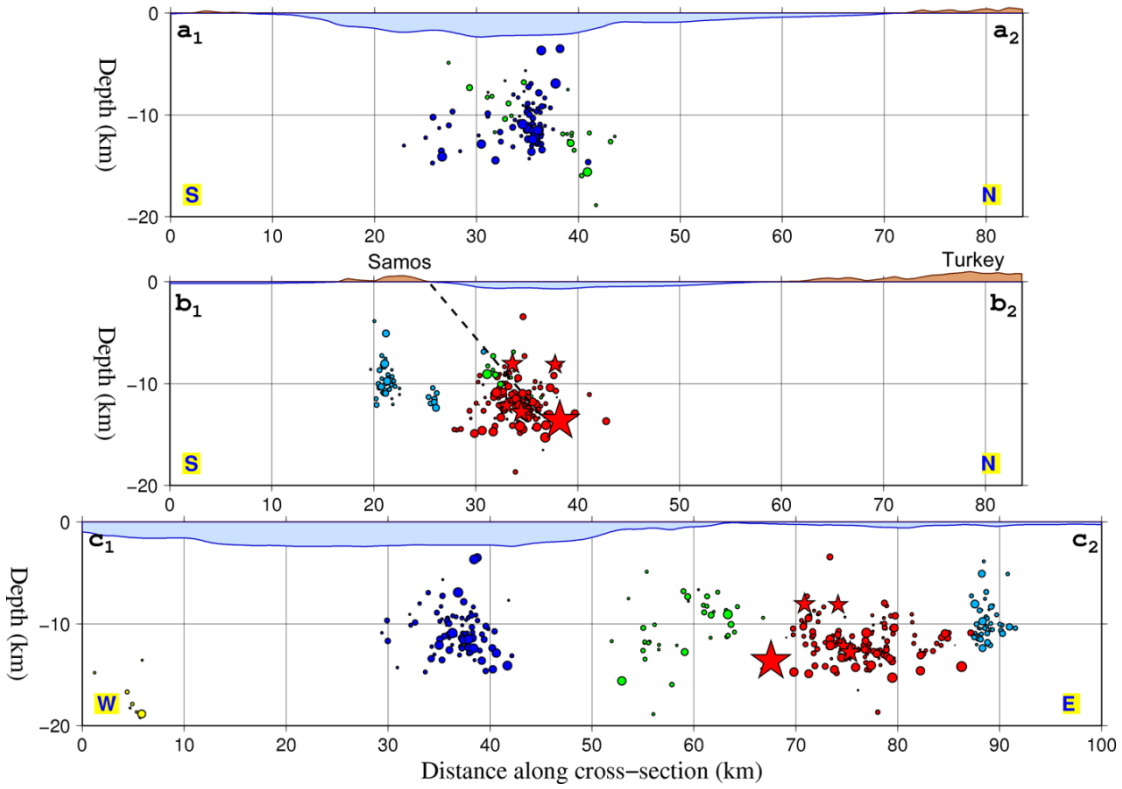

Figure 11: Cross-sections in a S-N (a_1-a_2, b_1-b_2) and W-E direction (c_1-c_2) along the profiles presented by dashed rectangles on the map of Fig. 10. Topography and bathymetry at the top of the cross-sections have been vertically exaggerated by ×2. The major events with M≥4.5 are depicted by stars.

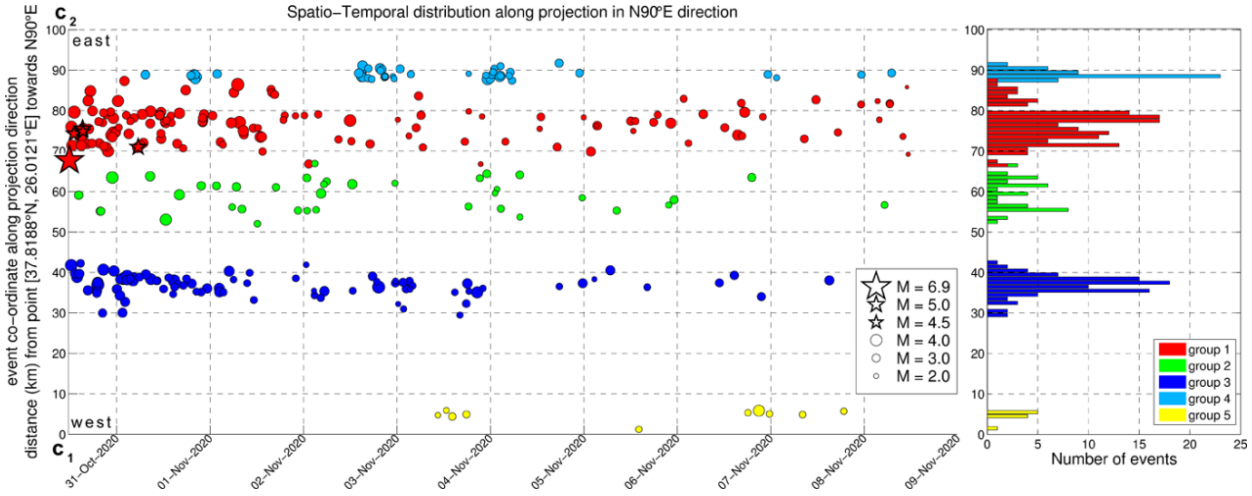

Figure 12: Spatiotemporal projection of the 2020 Samos aftershocks epicenters along the W-E profile c_1-c_2 of Fig. 10. The histogram on the right shows the number of aftershocks along the profile. The major events with M≥4.5 are depicted by stars.

The temporal evolution of the 2020 Samos aftershock sequence, until 08/11/2020, is presented in Fig. 12. Soon after the occurrence of the mainshock, the whole zone of groups 1-3 was activated, with most

aftershocks occurring in group 1, east of the mainshock. During the first hours, the activity was limited to a total length of approximately 40 km (from 40 to 80 km in the vertical axis of Fig. 12), but as the sequence evolved it apparently gradually extended to ~60 km in the E-W direction. Group 4 (cyan) at the eastern part of Samos Island, notably south of the main aftershock zone, was activated on 31 October with a few events, while two distinct bursts occurred during 2-4 November 2020. The isolated group 5 (yellow) presented some activity on 3 and 6-7 November. No aftershocks with M≥4.5 were recorded after 31 October 2020. The activity of the aftershock sequence appears to be gradually diminishing, so far without any major secondary outbreak.

5.2. Aftershocks focal mechanisms

Following the mainshock, 28 large aftershocks with M_w≥3.7 were processed to determine their focal mechanisms (Fig. 13). Initial solutions were estimated by an automated version of the method used to obtain the mainshock's parameters. Each automatic solution is manually revised and the results are published online (www.geophysics.geol.uoa.gr). The focal mechanism of the largest aftershock that occurred a few hours after the main event (30/10/2020 15:14:57 UTC), with M_w=5.0, resembles that of the mainshock, i.e. φ_1=264º, δ_1=37º, λ_1=-126º with a centroid depth of 15.0 km.

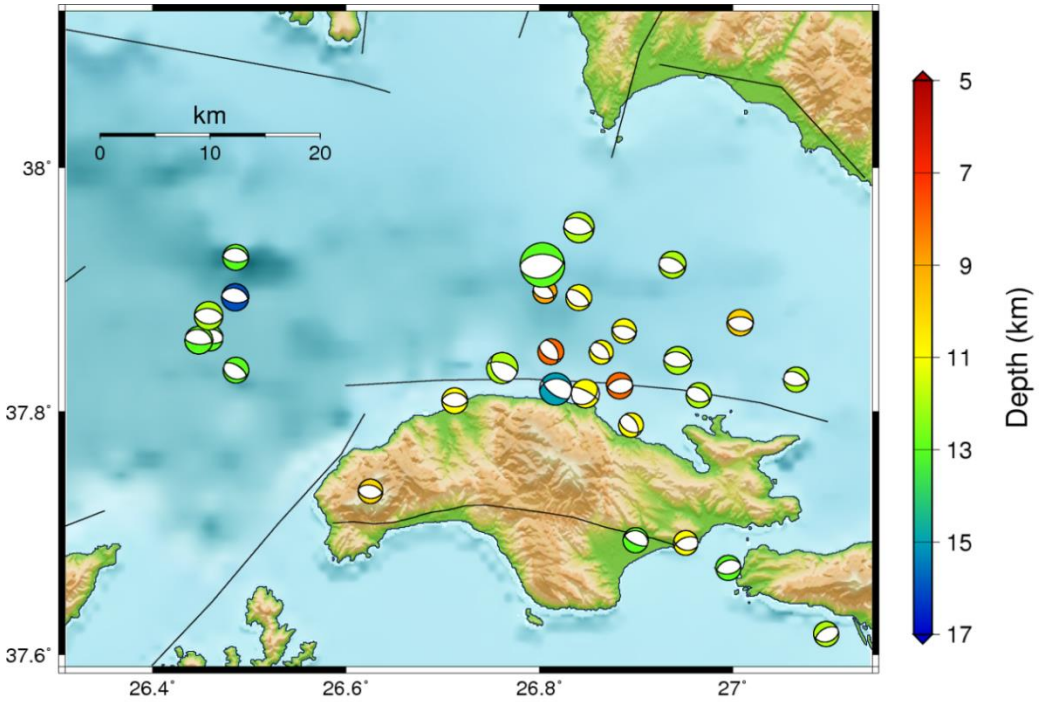

Figure 13: Focal mechanisms of the 2020 Samos mainshock and 28 major aftershocks (M_w≥3.7). Beachball locations are from the preliminary epicentral locations of routine analysis.

The average source parameters for the aftershocks, as determined from the distribution of strike, dip and rake angles, seem to agree with the modeling results for the mainshock, indicating E-W to WNW-ESE, almost pure dip-slip normal faulting

To obtain a preliminary estimate of the stress state related to the sequence, we employed the fast stress inversion method of Vavryčuk (2014), which performs iterative joint inversions of stress and fault orientations. The parameters of the principal stress axes for the optimal stress tensor were estimated: $\mathbf{S}_1$ (N304ºE/85º), $\mathbf{S}_2$ (N104ºE/4º) and $\mathbf{S}_3$ (N194ºE/2º), with an expected focal mechanism for optimally oriented faults with parameters φ_1=287º, δ_1=54º, λ_1=-85º for the north-dipping nodal plane and φ_2=99º,

δ_2=36º, λ_2=-97º for the south-dipping one. These results are in agreement with the data-driven stress model produced by Kapetanidis & Kassaras (2019) for the area (east of Samos Island, in particular), insinuating that fault kinematics of the current seismic sequence are consistent with those expected for a north-dipping fault plane, given the regional stress regime as determined from the focal mechanisms of past earthquakes.

5.3. Coulomb stress changes

Herein we present a preliminary model of Coulomb Failure Function changes (ΔCFF) to examine the pattern of stress transfer due to the displacement caused by the M_w=6.9 mainshock. The ΔCFF model was determined using the Coulomb 3.3 software (Toda *et al.*, 2011), for a fault with dimensions L=30 km, W=23 km and net slip u=1100 mm, with an effective coefficient of friction μ=0.4, taking into account the focal mechanism solution for the north-dipping nodal plane (φ_1=270º, δ_1=50º, λ_1=-81º; Fig. 6) and the seismic moment magnitude M_w=6.9.

Fig. 14 presents the ΔCFF distribution for a horizontal slice of the model at a depth of 11 km, for receiver faults with the same kinematics as that of the mainshock. The Coulomb stress transfer distribution shows that the positive lobes (stress load; red) are spread to the west and to the east or the fault plane, while the negative lobes (stress shadow; blue) cover the regions to the north and to the south. This result indicates that, for the given configuration, the mainshock can trigger seismicity at the western and eastern edges of the main rupture surface. Even a simplified model such as this can explain the activity at the spatial group 3 (Fig. 10; blue).

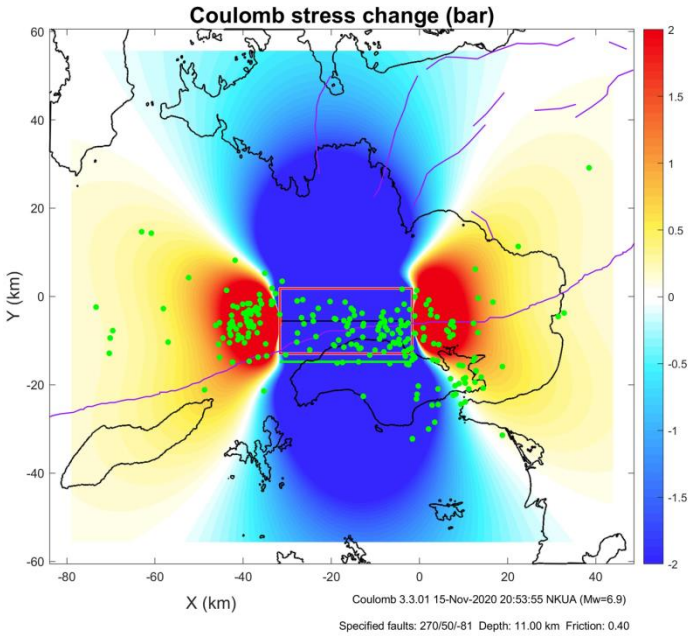

Figure 14: ΔCFF values for receiver faults of similar kinematics as that of the mainshock at the depth of 11 km. The red rectangle shows the projection of the fault plane on the surface. Red lobes indicate stress load while blue regions depict stress shadows. Green dots show the epicenters of aftershocks from the preliminary catalogue of routine locations at SL-NKUA. Purple lines are active faults (Ganas *et al.*, 2018).

6. Macroseismic effects of the 2020 Samos earthquake

6.1. Tsunami

A tsunami was generated by the Samos 2020 mainshock, producing minor damage at the surrounding coasts and especially in the towns of Vathy - Samos (Greece) and Sigacik (Turkey) (Fig. 15). Water inundating through streets and ports in the region was reported in the social media, along with tsunami warnings being issued for the Dodecanese islands in Greece. Heights of the tsunami from this event were larger than those of similar magnitude earthquakes in this region (Dağ, 2020). At the waterfront of Seferihisar, flooding reached heights of 1.9 m, causing one fatality; in Akarca, the tsunami reached heights of 6 m, penetrating 0.8 km inland; in Azmak, the tsunami penetrated 1.3 km inland and in Sigacik 0.32 km (Dağ, 2020).

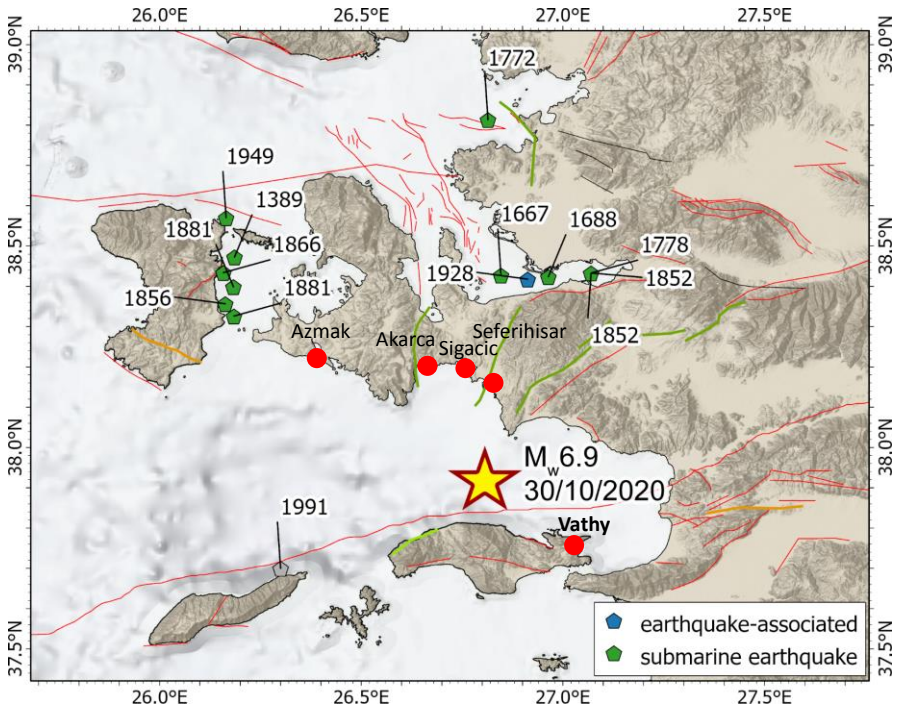

Figure 15. Locations of tsunamis observed during the mainshock (red solid circles, https://en.wikipedia.org/wiki/2020_Aegean_Sea_earthquake#Tsunami). Historical tsunamis (solid polygons) observed in the epicentral area (Papadopoulos, 2001). From the New Seismotectonic Atlas of Greece (Kassaras *et al.*, 2020; http://www.geophysics.geol.uoa.gr/atlas.html)

6.2. Structural effects

During the main seismic event of October 30th 2020, damage occurred to a number of structures, mainly old buildings and monumental structures (Fig. 16). In general, considering the high intensity of the earthquake (Fig. 8) with Spectral Accelerations (SA) up to 0.6 g for periods within the 0.01-0.3 s range (www.itsak.gr), the buildings on Samos Island behaved well. This range is close to the eigenperiod of most of the buildings, since over 99% of them have up to three storeys according to the 2011 building census data. The majority of the building stock in the island suffered minor damage, even though 70% of buildings were constructed before 1985, and thus, with low earthquake-resistant design (1959 seismic code) compared to the post-1985 codes, which includes EC8 (CEN, 2004). The overall satisfactory

structural performance can be attributed to the good construction quality. Damage of non-structural components was also evident in the areas of Samos Island with the highest observed intensities.

As far as the school buildings are concerned, until now, from the reports of the authorities, out of the 44 school units inspected, 11 have suffered extensive damage. It should be noted that most schools in Samos Island (about 80%) were constructed before 1985 and that only about 30% of school buildings are made from reinforced concrete. Some monumental structures, temples and churches also faced significant damages. More specifically, over 60 churches on the island were severely damaged by the earthquake. In the area of eastern Samos, 24 churches suffered significant damage. In west Samos, 30 churches were also damaged.

Figure 16. Structural damage in Samos (Vathy) due to the mainshock (from various sources in the web).

The acceleration response spectra of the recorded accelerations (www.itsak.gr) show that the high-rise buildings (4-6 storeys), were subjected to accelerations up to 1 g. This could be one of the reasons why the high-rise buildings in Izmir suffered more significant damages compared to the low to mid-rise buildings in Samos Island (Fig. 17). Of course, there are also other reasons, like the frequency content and the directivity of the excitations, the quality of the foundation soil, the constructions, etc.

Figure 17. Structural damage in Izmir due to the mainshock (from various sources in the web).

7. Summary - Discussion

The 2020 Samos earthquake was one of the strongest events to occur in Greece during the last decades. However, considering its magnitude (M_w=6.9) and the fault's proximity to the island, Samos suffered relatively low damage compared to Izmir, located at a much further distance of ~75 km from the mainshock's epicenter. One of the main issues with such earthquakes, i.e. occurring offshore and exhibiting normal faulting, as was also the case of the 2017 Kos (Ganas *et al.*, 2019) or the 2017 Lesvos (Papadimitriou *et al.*, 2018) events, is the determination of the fault plane out of the two nodal planes of the focal mechanism. The deformation pattern (Fig. 7) greatly aids to resolve this ambiguity, as the preliminary results indicate that the western part of Samos Island was uplifted, while subsidence was observed at the northern edge of the central part of the island. Taking also into account the distribution of the relocated hypocenters (Fig. 11, b_1-b_2), a north-dipping fault plane can be inferred for the mainshock. This places most of Samos Island on the footwall, which is another factor that may have lowered the damage potential of the earthquake on the island.

The spatial distribution of hypocenters presents similarities with that of the 2017 Kos earthquake (Ganas *et al.*, 2019), in the sense that the eastern part of the aftershocks sequence was more densely populated with events than the western part, while a significant lack of aftershocks is observed between the two halves. This gap could coincide with the region of the fault surface where most of the co-seismic slip occurred, i.e. a large asperity that broke during the mainshock, thus only few aftershocks are observed therein (spatial group 2; Fig. 10). On the other hand, the Coulomb stress transfer pattern for this type of event and for receiver faults of similar kinematics (Fig. 14) shows that stress load is transferred to the eastern and western edges of the rupture plane. This can explain triggering of aftershocks in spatial groups 3 and 5 in the west (Fig. 10), but also group 4 in the eastern part of the island. The latter almost certainly belongs to a different fault than the one of the mainshock which could be related to some of the mapped structures observed on the island (Fig. 2).

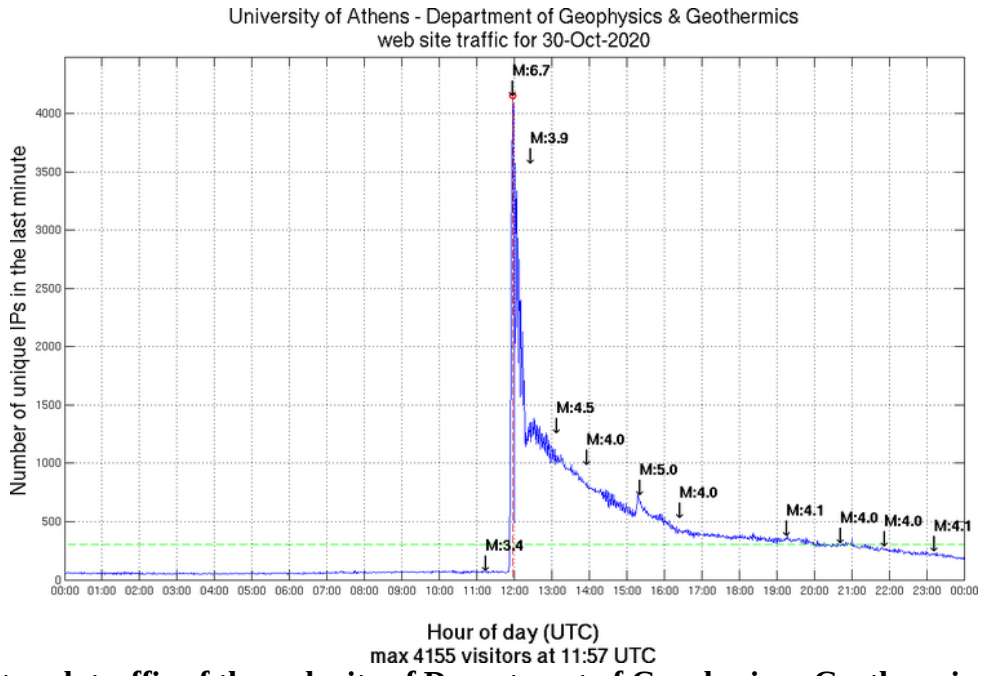

Figure 18: Network traffic of the web-site of Department of Geophysics - Geothermics on 30 October 2020. Shortly after the mainshock occurred (at 11:51:28 UTC) a surge of over 4,000 unique visitors within 1 minute was recorded.
(http://www.geophysics.geol.uoa.gr/stations/traffic/index3.php?date=20201030&lng=en)

The complex nature of this earthquake's source was indicated during our attempts to determine the mainshock's moment tensor. A more detailed investigation of its co-seismic slip model could reveal if indeed a large asperity broke in the region where the gap in the aftershocks distribution is observed, as well as whether the mainshock in fact ruptured two distinct fault segments in cascade, producing a total seismic moment equivalent to M_w=6.9. The latter could explain why the largest aftershock is of the order of M_w=5.0 and not M_w≈6.0, as would be expected for a mainshock of M_w≈7.0, had it occurred on a single large fault.

It is worth noting that the mainshock was automatically detected and reported at the web-site of the Section of Geophysics-Geothermics at the National and Kapodistrian University of Athens, which reached network traffic of over 4,000 unique IPs per minute, about 6 minutes after the mainshock's occurrence (Fig. 18). In addition, a dedicated interactive web-page has been created for the monitoring of the 2020 Samos aftershock sequence (Fig. 19), where the user can also view fault sources from the European Database of Seismogenic Faults (EDSF, Basili *et al.*, 2009; Woessner *et al.*, 2015), past seismicity (Makropoulos *et al.*, 2012), focal mechanisms determined at SL-NKUA and also view real-time waveforms of local and regional HUSN stations.

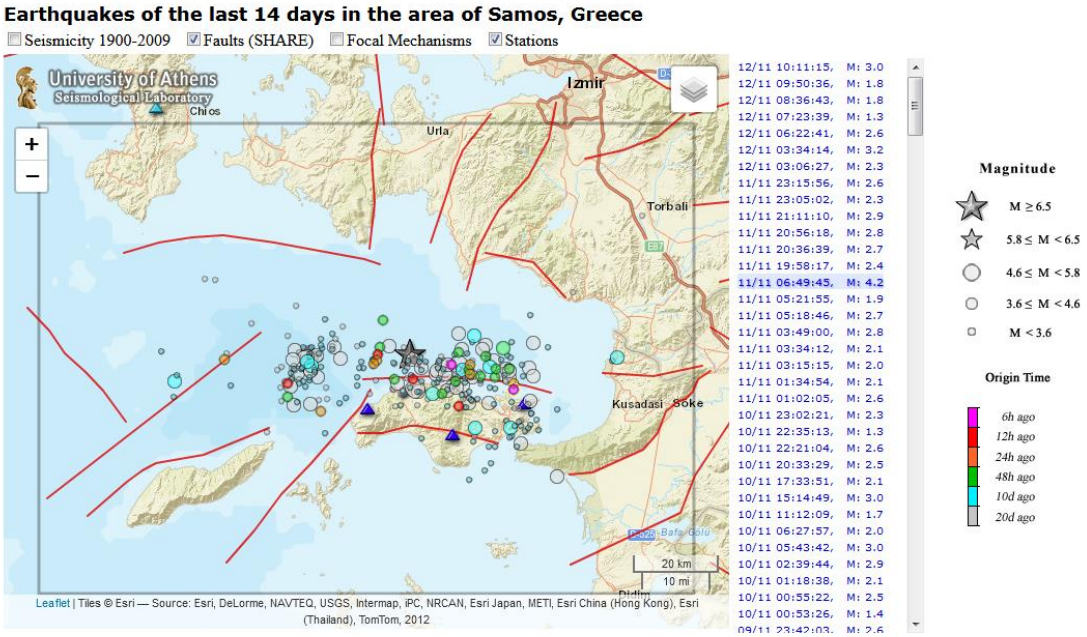

Click on headers to sort table

#	Sol. Type	Origin Time (GMT)	Epicentral Location	Latitude (°N)	Longitude (°E)	Depth (km)	Mag.
1	M	12/11/2020 10:11:15	5.0 km NNE of Samos	37.7983	26.9990	11.0	3.0
2	M	12/11/2020 09:50:36	16.3 km NW of Samos	37.8515	26.8350	16.0	1.8
3	M	12/11/2020 08:36:43	22.7 km WNW of Samos	37.8210	26.7312	8.0	1.8
4	M	12/11/2020 07:23:39	32.4 km WNW of Samos	37.8725	26.6383	12.0	1.3
5	M	12/11/2020 06:22:41	32.7 km NE of Ikaria	37.8112	26.4012	2.0	2.6
6	M	12/11/2020 03:34:14	10.9 km W of Samos	37.7648	26.8528	12.0	3.2

Figure 19: Interactive web-page for the seismicity in the 2020 Samos aftershock zone, automatically detected and manually analyzed at SL-NKUA. (http://www.geophysics.geol.uoa.gr/stations/gmaps3/samos_leaf.php?lng=en)

References

Allen, T.I. & Wald, D.J., 2009. On the Use of High-Resolution Topographic Data as a Proxy for Seismic Site Conditions (VS30). Bull. Seismol. Soc. Am. 99, 935–943. doi:10.1785/0120080255

Ambraseys, N., 2009. Earthquakes in the Mediterranean and Middle East: a multidisciplinary study of seismicity up to 1900. Cambridge University Press

Basili, R., Kastelic, V., Valensise, G., Group & the DW, 2009. DISS3 tutorial series: guidelines for compiling records of the database of the individual seismogenic sources, version 3. INGV.

Bossu, R., Roussel, F., Fallou, L., Landès, M., Steed, R., Mazet-Roux, G., Dupont, A., Frobert, L. & Petersen, L., 2018. LastQuake: From rapid information to global seismic risk reduction. Int. J. Disaster Risk Reduct. 28, 32–42. doi:10.1016/j.ijdrr.2018.02.024

Bouchon, M., 1979. Discrete wave number representation of elastic wave fields in three-space dimension, J. Geophys. Res., 84, 3609–3614.

Bouchon, M., 2003. A review of the discrete wavenumber method, Pure Appl. Geophys., 160, 445–465.

CEN, 2004. Eurocode 8: Design of structures for earthquake resistance - Part 1: General rules, seismic actions and rules for buildings, European Standard EN 1998-1:2004. Brussels, Belgium: European Committee for Standardisation.

Dağ, B., 2020. "Turkey sees larger tsunami after latest quake". Anadolu Agency. Retrieved 9 November 2020.

Ganas, A., Tsironi, V., Kollia, E., Delagas, M., Tsimi, C. & Oikonomou, A., 2018. Recent upgrades of the NOA database of active faults in Greece (NOAFAULTs). In Proceedings of the 19th General Assembly of WEGENER, Grenoble, France, 10–13 September 2018.

Ganas, A., Elias, P., Kapetanidis, V., Valkaniotis, S., Briole, P., Kassaras, I., *et al.*, 2019. The July 20, 2017 M6.6 Kos Earthquake: Seismic and Geodetic Evidence for an Active North-Dipping Normal Fault at the Western End of the Gulf of Gökova (SE Aegean Sea). Pure Appl. Geophys. 176, 4177–4211. doi:10.1007/s00024-019-02154-y

Gasperini, P., Vannucci, G., Tripone, D. & Boschi, E., 2010. The location and sizing of historical earthquakes using the attenuation of macroseismic intensity with distance. Bull. Seismol. Soc. Am., 100, 2035–2066.

Genç, C.Ş., Altunkaynak, Ş., Karacık, Z., Yazman, M. & Yılmaz, Y., 2001. The Çubukludağ graben, south of İzmir: its tectonic significance in the Neogene geological evolution of the western Anatolia, Geodin. Acta 14, 1-3, 45-55, doi: 10.1016/S0985-3111(00)01061-5.

Gürer, Ö.F., Sanğu, E., Özburan, M., Gürbüz, A., Sarica-Filoreau, N., 2013. Complex basin evolution in the Gökova Gulf region: implications on the Late Cenozoic tectonics of southwest Turkey. Int. J. Earth Sci. 102, 2199–2221. doi:10.1007/s00531-013-0909-1

Jolivet, L. & Brun, J.-P, 2010. Cenozoic geodynamic evolution of the Aegean. Int. J. Earth Sci. 99, 109–138.

Kapetanidis, V., Kassaras, I., 2019. Contemporary crustal stress of the Greek region deduced from earthquake focal mechanisms. J. Geodyn. 123, 55–82. doi:10.1016/j.jog.2018.11.004

Karakonstantis, A., 2017. 3-D simulation of crust and upper mantle structure in the broader Hellenic area through Seismic Tomography, Ph D. Thesis, Department of Geophysics-Geothermics, Faculty of Geology, University of Athens, Greece (in Greek).

Karakostas, V.G., Papadimitriou, E.E., Karakaisis, G.F., Papazachos, C.B., Scordilis, E.M. Vargemezis, G. & Aidona, E., 2003. The 2001 Skyros, Northern Aegean, Greece, earthquake sequence: off-fault aftershocks, tectonic implications, and seismicity triggering, Geophys. Res. Lett. 30, 1, 12-1-12-4, doi: 10.1029/2002GL015814.

Kassaras, I., Kapetanidis, V., Ganas, A., Tzanis, A., Kosma, C., Karakonstantis, A., Valkaniotis, S., Chailas, S., Kouskouna, V. & Papadimitriou, P., 2020. The New Seismotectonic Atlas of Greece (v1.0) and Its Implementation. Geosciences 10, 447. doi:10.3390/geosciences10110447

Kaviris, G., Papadimitriou, P., Kravvariti, Ph., Kapetanidis, V., Karakonstantis, A., Voulgaris, N., Makropoulos, K., 2015. A detailed seismic anisotropy study during the 2011–2012 unrest period in the Santorini Volcanic Complex. Physics of the Earth and Planetary Interiors, 238, 51–88.

Klein, F.W., 2002. User's guide to HYPOINVERSE-2000: a Fortran program to solve for earthquake locations and magnitudes, U.S. Geol. Surv. Prof. Pap., rep. 02-17, 1–123.

Kouskouna, V. & Sakkas, G., 2013. The University of Athens Hellenic Macroseismic Database (HMDB.UoA): historical earth- quakes. J. Seismol., 17, 1253–1280. https://doi.org/10.1007 /s10950-013-9390-3

Kurtuluş, C., Doğan, B., Sertçelik, F., Canbay, M. & Küçük, H.M., 2009. Determination of the tectonic evolution of the Edremit Gulf based on seismic reflection studies. Mar. Geophys. Res. 30, 121–134. doi:10.1007/s11001-009-9072-2

Locati, M., Rovida, A., Albini, P. & Stucchi, M., 2014. The AHEAD Portal: a gateway to European Historical Earthquake Data. Seismol. Res. Lett., 85, 727–734. https://doi.org/10.1785 /0220130113

Makropoulos, K., Kaviris, G. & Kouskouna, V., 2012. An updated and extended earthquake catalogue for Greece and adjacent areas since 1900, Nat. Hazards Earth Syst. Sci., 12, 1425-1430.

Malandri, C., Soukis, K., Maffione, M., Özkaptan, M., Vassilakis, E., Lozios, S. & van Hinsbergen, D.J.J., 2017. Vertical-axis rotations accommodated along the Mid-Cycladic lineament on Paros Island in the extensional heart of the Aegean orocline (Greece). Lithosphere 9, 78–99. doi:10.1130/L575.1

Mascle, J. & Martin, L., 1990. Shallow structure recent evolution of the Aegean Sea: a synthesis based on continuous reflection profiles. Marine Geology 94, 271– 299.

McKenzie, D., 1972. Active tectonics of the Mediterranean region. Geophys. J. Roy. Astr. Soc. 30, 2,109-185, doi: 10.1111/j.1365-246X.1972.tb02351.x.

McKenzie, D., 1978. Active tectonics of the Alpine-Himalayan belt: the Aegean Sea and surrounding regions. Geophys. J. R. Astr. Soc. 55, 217–254.

Mercier, J.L., Sorel, D., Vergely, P. and Simeakis, K. (1989), Extensional tectonic regimes in the Aegean basins during the Cenozoic. Basin Research, 2: 49-71. https://doi.org/10.1111/j.1365-2117.1989.tb00026.x

Ocakoğlu, N., Demirbag, E. & Kuşçu, İ., 2004. Neotectonic structures in the area offshore of Alaçati, Doğanbey and Kuşadası (western Turkey): evidence of strike-slip faulting in the Aegean extensional province, Tectonophysics 391, 1-4, 67-83, DOI: 10.1016/j.tecto.2004.07.008.

Papadimitriou, P., Chousianitis, K., Agalos, A., *et al.*, 2012. The spatially extended 2006 April Zakynthos (Ionian Islands, Greece) seismic sequence and evidence for stress transfer, Geophys. Jour. Intern., 190 (2), 1025-1040.

Papadimitriou, P., Kapetanidis, V., Karakonstantis, A., Kaviris, G., Voulgaris, N. & Makropoulos, K., 2015. The Santorini Volcanic Complex: A detailed multi-parameter seismological approach with emphasis on the 2011–2012 unrest period. J. Geodyn., 85, 32–57.

Papadimitriou, P., Kassaras, I., Kaviris, G., Tselentis, G.-A., Voulgaris, N., Lekkas, E., Chouliaras, G., Evangelidis, C., Pavlou, K., Kapetanidis, V., Karakonstantis, A., Kazantzidou-Firtinidou, D., Fountoulakis, I., Millas, C., Spingos, I., Aspiotis, T., Moumoulidou, A., Skourtsos, E., Antoniou, V., Andreadakis, E., Mavroulis, S. & Kleanthi, M., 2018. The 12th June 2017 M_w = 6.3 Lesvos earthquake from detailed seismological observations. J. Geodyn. 115, 23–42. doi:10.1016/j.jog.2018.01.009

Papadimitriou, P., Kapetanidis, V., Karakonstantis, A., Spingos, I., Pavlou, K., Kaviris, G., Kassaras, I., Sakkas, V. & Voulgaris, N., 2020. The 25 October, 2018 Zakynthos (Greece) earthquake: seismic activity at the transition between a transform fault and a subduction zone, GJI-19-0844. (*submitted to Geophys. J. Int.*)

Papadopoulos, G.A., 2001. Tsunamis in the east Mediterranean: 1. A catalogue for the area of Greece and adjacent seas. In: proceedings of the "Joint IOC - IUGG International Workshop: Tsunami Risk Assessment Beyond 2000: Theory, Practice and Plans, Moscow, June 14-16, 2000", pp. 34-43.

Papazachos, B.C. & Papazachou, C., 2003. The earthquakes of Greece. Ziti Publ Co, Thessaloniki, Greece.

Pomonis, P. & Hatzipanagiotou, K., 1998. Petrography and geochemistry of relict peridotites of the Kallithea-Drakei area (W. Samos). Bull. Geol. Soc. Greece, 32, 215–224.

Ring, U., Okrusch, M. & Will, T. 2007. Samos Island, Part I: metamorphosed and non-metamorphosed nappes, and sedimentary basins. In: (Eds.) Gordon Lister, Marnie Forster, and Uwe Ring, Inside the Aegean Metamorphic Core Complexes, Journal of the Virtual Explorer, Electronic Edition, ISSN 1441-8142, volume 27, paper 5, doi:10.3809/jvirtex.2007.00180

Roumelioti, Z., Kiratzi, A. & Melis, N., 2003. Relocation of the 26 July 2001 Skyros Island (Greece) earthquake sequence using the double-difference technique. Physics of the Earth and Planetary Interiors, 138(3-4), 231–239. doi:10.1016/s0031-9201(03)00138-9

Stucchi, M., Rovida, A., Gomez Capera, A.A., Alexandre, P., Camelbeeck, T., Demircioglu, M.B., Gasperini, P., Kouskouna, V., Musson, R.M.W., Radulian, M., Sesetyan, K., Vilanova, S., Baumont, D., Bungum, H., Fäh, D., Lenhardt, W., Makropoulos, K., Martinez Solares, J.M., Scotti, O.,Zivcic, M., Albini, P., Batllo, J., Papaioannou, C., Tatevossian, R., Locati, M., Meletti, C., Viganò, D. & Giardini, D., 2013. The SHARE European Earthquake Catalog (SHEEC) 1000–18 99, J. Seismolog., 17 (2), 523–544.

Tan, O., Papadimitriou, E.E., Pabucçu, Z., Karakostas, V., Yörük, A. & Leptokaropoulos, K., 2014. A detailed analysis of microseismicity in Samos and Kusadasi (Eastern Aegean Sea) areas. Acta Geophys. 62, 1283–1309. doi:10.2478/s11600-013-0194-1

Taxeidis K., 2003. Study of Historical Seismicity of the Eastern Aegean Islands. PhD thesis, NKUA, Greece, 301 pp.

Toda, S., Stein, R.S., Sevilgen, V. & Lin, J., 2011. Coulomb 3.3 Graphic-rich deformation and stress-change software for earthquake, tectonic, and volcano research and teaching-user guide. U.S. Geological Survey Open-File Report 2011-1060. pp. 63. http://pubs.usgs.gov/of/2011/1060/.

USGS, 2017. ShakeMap – Earthquake Ground Motion and Shaking Intensity Maps: U.S. Geological Survey, https://doi.org/10.5066/F7W957B2.

Vavryčuk, V., 2014. Iterative joint inversion for stress and fault orientations from focal mechanisms. Geophys. J. Int. 199, 69–77. doi:10.1093/gji/ggu224

Waldhauser, F., 2001. hypoDD-A Program to Compute Double-Difference Hypocenter Locations, U.S. Geol. Surv. Open File Rep. 01-113, 25 p.

Woessner, J., Danciu, L., Giardini, D., Crowley, H., Cotton, F., Grünthal, G., Valensise, G., Arvidsson, R., Basili, R., Demircioglu, M.B., Hiemer, S., Meletti, C., Musson, R.W., Rovida, A.N., Sesetyan, K., Stucchi M. & the SHARE Consortium, 2015. The 2013 European Seismic Hazard Model: key components and results. Bull Earthquake Eng 13, 3553–3596 (2015). https://doi.org/10.1007/s10518-015-9795-1.